Geophysical Research Letters

RESEARCH LETTER
10.1029/2023GL104717

Key Points:

- Elastic radiation of analogue experimental volcanic subsonic to supersonic jets was compared against high-speed shadowgraph analysis
- We quantified variation in the spectral features, energy partitioning and jet structure due to differences in conduit roughness
- Different behavior in subsonic versus supersonic regime was observed due to distinct dominating noise sources at different roughness

Supporting Information:

Supporting Information may be found in the online version of this article.

Correspondence to:

L. Spina,
laura.spina@ingv.it

Citation:

Spina, L., Taddeucci, J., Pennacchia, F., Morgavi, D., Peña Fernández, J. J., Sesterhenn, J., et al. (2023). The effect of conduit walls roughness on volcanic jets and their seismo-acoustic radiation: An experimental investigation. *Geophysical Research Letters*, *50*, e2023GL104717. https://doi.org/10.1029/2023GL104717

Received 31 MAY 2023
Accepted 13 SEP 2023

Author Contributions:

Conceptualization: Laura Spina, Jacopo Taddeucci, Daniele Morgavi, Piergiorgio Scarlato
Data curation: Laura Spina, Jacopo Taddeucci
Formal analysis: Laura Spina, Jacopo Taddeucci, Daniele Morgavi
Funding acquisition: Laura Spina, Jacopo Taddeucci, Piergiorgio Scarlato
Investigation: Laura Spina, Jacopo Taddeucci

The Effect of Conduit Walls Roughness on Volcanic Jets and Their Seismo-Acoustic Radiation: An Experimental Investigation

Laura Spina[1], Jacopo Taddeucci[1], Francesco Pennacchia[1], Daniele Morgavi[2], Juan José Peña Fernández[3], Jörn Sesterhenn[4], Giuseppe La Spina[5], and Piergiorgio Scarlato[1]

[1]Istituto Nazionale di Geofisica e Vulcanologia, Sezione di Roma1, Rome, Italy, [2]Dipartimento di Scienze della Terra, dell'Ambiente e delle Risorse (DiSTAR), Università Degli Studi di Napoli Federico II, Napoli, Italy, [3]Department of Earth and Environmental Sciences, Ludwig-Maximilians-Universität (LMU) Munich, Munich, Germany, [4]Universität Bayreuth, Fakultät für Ingenieurwissenschaften, Bayreuth, Germany, [5]Istituto Nazionale di Geofisica e Vulcanologia, Osservatorio Etneo, Catania, Italy

Abstract To explore the effect of conduit roughness on volcanic jet dynamics and on the related seismo-acoustic radiation we performed a series of shock-tube experiments using pipes with variable inner surface fractal dimension *D*. Variable starting pressure produced subsonic to supersonic jets visualized using high-speed shadowgraph and recorded with an array of accelerometers and microphones. At all starting pressures, increasing *D* increases the energy transfer from the gas to the conduit walls, decreasing the jet exit velocity (Mach number) and, for supersonic cases, the related shock-cell spacing, and increasing the seismic to acoustic radiation amplitude ratio. The roughness-induced changes in jet velocity and turbulence affect the dominant sources of the jet noise and modulates the spectral properties of the acoustic signals. From our study we show that conduit wall roughness is an important and yet largely neglected factor in the dynamics of explosive volcanic eruptions and their monitored geophysical signals.

Plain Language Summary Volcanoes are amongst the most fascinating and mysterious subjects of science, for they allow no direct observation of what is happening within the conduit during eruptive activity. Indirect observations (such as measurements of the sound and vibration accompanying eruptions) are routinely performed for monitoring and research purposes. Laboratory studies mimicking the eruptive processes in small-scale devices, are of great support for correctly interpreting such data. As such, we investigated the effect of the irregularity of conduit surface, amongst the most relevant and poorly known variables characterizing the eruptive processes, on volcanic jets and on their seismic and acoustic signals. We performed a series of laboratory experiments using conduits with different roughness of the internal surface and various starting pressures. Microphones and accelerometers, capable of measuring conduit sounds and vibration, respectively, in synch with high-speed camera were used to constrain the characteristics of the generated subsonic and supersonic jets. Results show that conduit roughness controls: (a) the relative amplitude of seismic and acoustic signals; (b) the velocity, turbulence and properties of the sound of these jets. Our results will shed light on the link between observation at the surface and dynamic evolution of conduit geometry at depth.

1. Introduction

Explosive volcanic eruptions generate jet flow by the impulsive release of gas and pyroclasts mixtures in the atmosphere (e.g., Matoza et al., 2009; Wilson, 1976). The dynamics of volcanic jets control eruption evolution, its hazards, and the seismo-acoustic signals used to monitor it (e.g., Haney et al., 2018; Matoza et al., 2013; Prejean & Brodsky, 2011), but how such dynamics are affected by the flow of the gas-pyroclasts mixture in the conduit is still unclear.

Impulsive discharge of gas from a pressurized reservoir generates a compressive wave, followed by the formation of vortex rings and a trailing jet, with specific acoustic signatures (e.g., Pena Fernandez et al., 2020). At the shear layer between the jet and the surrounding static fluid, turbulent mixing generates large and fine scale vorticity ensuing turbulent mixing noise. In supersonic jets the mismatch between static pressure inside and outside the jet produces quasi-periodic shock-cells that interact with the turbulence structure in the shear layer, producing a characteristic broadband shock noise and screech tones (e.g., Norman & Winkler, 1985; Peña Fernández &

Methodology: Laura Spina, Jacopo Taddeucci, Francesco Pennacchia, Juan José Peña Fernández, Jörn Sesterhenn, Giuseppe La Spina
Project Administration: Laura Spina, Jacopo Taddeucci
Resources: Laura Spina, Jacopo Taddeucci, Daniele Morgavi, Piergiorgio Scarlato
Software: Laura Spina, Jacopo Taddeucci
Supervision: Laura Spina, Jacopo Taddeucci
Validation: Laura Spina, Jacopo Taddeucci, Juan José Peña Fernández, Jörn Sesterhenn, Giuseppe La Spina
Visualization: Laura Spina, Jacopo Taddeucci
Writing – original draft: Laura Spina, Jacopo Taddeucci
Writing – review & editing: Laura Spina, Jacopo Taddeucci, Daniele Morgavi, Juan José Peña Fernández, Jörn Sesterhenn, Giuseppe La Spina, Piergiorgio Scarlato

Sesterhenn, 2017; Tam et al., 2008). Jet noise from volcanoes possesses additional complexities, due to the multiphase nature of the released fluid and to the complexity of crater and conduit morphology, with implications on the directivity of the radiated acoustic signals (e.g., Genco et al., 2014; Matoza et al., 2013; Pena-Fernandez et al., 2020; Taddeucci et al., 2012, 2014). Additionally, exploring the nature of volcanic jets and of jet noise requires addressing the audible components of the acoustic signals that have been recently the object of a renewed interest (e.g., Goto et al., 2014; Matoza et al., 2019, 2022; Rowell et al., 2014; Taddeucci et al., 2021). Yet fundamental source parameters can be derived from the observation of jet noise features of volcanic explosion; as an example Mach flow number (hence jet velocity) and vent diameter have been inferred from the observation of jet noise and high-speed video of vortex ring originating from gas-rich jets at Stromboli (Italy; Taddeucci et al., 2021).

Laboratory jets have indicated that the initial condition of the jet influences the downstream development (hence structures) through the entire flow field (e.g., George, 1989; Mi et al., 2001). High values of conduit length to diameter ratio, as in volcanic explosion occurring at depth, increase the thickness of the initial shear layer: for fixed diameters, the higher the length of the pipe the higher the initial thickness of the shear layer (e.g., Jothi & Srinivasan, 2009). Similarly, the geometrical properties of jet nozzle have been shown to modulate jet structures: amongst others the arrangement of chevrons at the nozzle (e.g., Bridges & Brown, 2004; Heeb et al., 2016), the geometry of the exit vent (e.g., Cigala et al., 2017; Schmid et al., 2022; Swanson et al., 2018), pipe surface roughness at the micron scale (e.g., Jothi & Srinivasan, 2013). Clearly, it is of paramount importance to map the effect of complex volcanic geometries on observable parameters through well-constrained aeroacoustics laboratory studies.

Here, for the first time we investigate through laboratory experiments how surface roughness of conduit walls reflects on volcanic jet properties and the related seismo-acoustic radiation. We performed a set of laboratory shock-tube experiments mimicking volcanic jets dynamics, by changing the pressure of the high-pressure reservoir and the roughness of the conduit surface, quantified by means of fractal dimension. The structure of the jet and the accelerometric and acoustic related wave field are investigated using high-speed imaging and through an array of accelerometric and acoustic sensors.

2. Experimental Methods

2.1. Experimental Setup

The experimental setup (Figure 1) consists of a shock tube composed by (a) a high-pressure reservoir, that is, a cylindrical polyethylene tube (78 cm long, 3.8 cm inner diameter, 8.8×10^{-4} m^3 inner volume), pressurized using compressed air at 2×10^5, 4×10^5, 6×10^5, 7×10^5, and 8×10^5 Pa, corresponding to pressure ratios (reservoir pressure divided by ambient pressure) of $P = 2$, 4, 6, 7, and 8; (b) an electrovalve allowing for rapid pressure release (<0.005 s); (c) the experimental analogue conduit, open to the atmosphere (80 cm long, 3 cm average inner diameter, 5.7×10^{-4} m^3 average inner volume). The opening of the electrovalve generates a shock wave that pressurizes the air in the analogue conduit, from which, depending on P, a subsonic or supersonic jet is released into the atmosphere whilst radiating elastic energy to the surrounding medium. To vary conduit surface roughness, we used three home-build epoxy pipes with the internal surface characterized by a different fractal dimension D: 2 (smooth surface), 2.18, and 2.99 (Spina et al., 2019, 2022; Giudicepietro et al., 2021 for further details).

The seismo-acoustic radiation was recorded along the conduit by accelerometers and in the atmosphere by microphones, respectively. A triaxial (frequency: 2 to 7 KHz sensitivity: 10 mV/g) and two monoaxial PCB Piezotronics accelerometers (frequency:0.5 to 10 KHz sensitivity: 100 mV/g) were placed in two slots along the conduit wall at ca. 7 (slot A) and 40 cm (slot B) below the outlet. The monoaxial accelerometers were alternated to the triaxial accelerometer, which was always located in slot B. We used two microphones: a PCB Piezotronics ICP 378B02 (frequency:7 Hz to 10 KHz sensitivity:50 mV/Pa in the band 7 Hz to 10 KHz (±1 dB) and ±2 dB in the range 3.75–20,000 Hz) and a GRAS 40AN (frequency: 0.5 Hz–20 KHz sensitivity: 50 mV/Pa) located at 30 cm left and right of the vent respectively (positions J and K). To avoid acoustic signal saturation, only for experiments with $D = 2$, an additional dataset of acoustic signals was acquired at a distance of 1 m (position L and N for the left and right side of the vent respectively; not included in Figure 1) and later corrected to the reference distance of 30 cm from the vent. Both accelerometric and acoustic signals were recorded at 200 KHz. In the rest of the paper only acoustic data from positions J and L and the accelerometric data from the monoaxial sensor

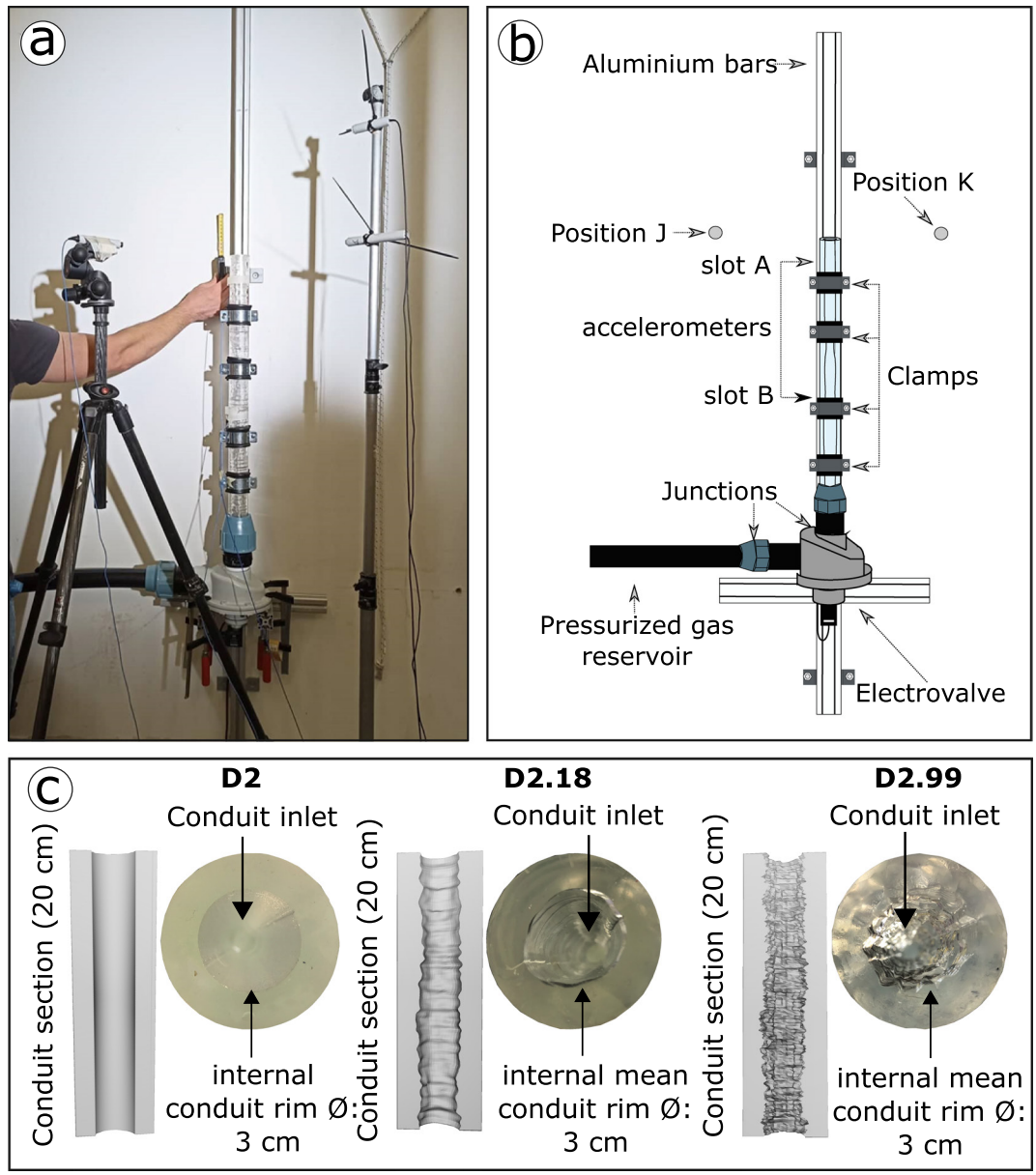

Figure 1. Experimental setup. (a) Picture and (b) schematic sketch; (c) longitudinal sections (20 cm long, left-hand image) and top views (right-hand image) of the fractal analogue conduits.

in slot B are shown, the other measurements providing congruent results (Figures S1–S6 in Supporting Information S1). A high-speed camera (NAC MEMRECAM HX-3) synchronized with accelerometric and acoustic sensors filmed the conduit outlet and the lower part of the jet at 30–50 KHz using shadowgraph and, for $P = 8$, Schlieren imaging (Davies, 1981) and background subtraction (Supporting Information S1). We performed more than 150 experiments spanning 15 different starting conditions in terms of D and P. Repeated experiments confirmed the full reproducibility of the observations. The experiments were not performed in an anechoic chamber; and acoustic reflections from the surroundings possibly entered the late part of our recordings. To limit this effect, as specified in Section 2.2, we mostly did not account for the coda waveforms of acoustic and accelerometric signals. Figure S1 in Supporting Information S1 displays examples of acoustic and accelerometric waveforms of subsonic ($P = 2$) and supersonic ($P = 8$) jets for $D = 2$. Velocity and displacement waveforms obtained by integration of a subsonic and supersonic accelerometric event are shown in Figure S2 in Supporting Information S1.

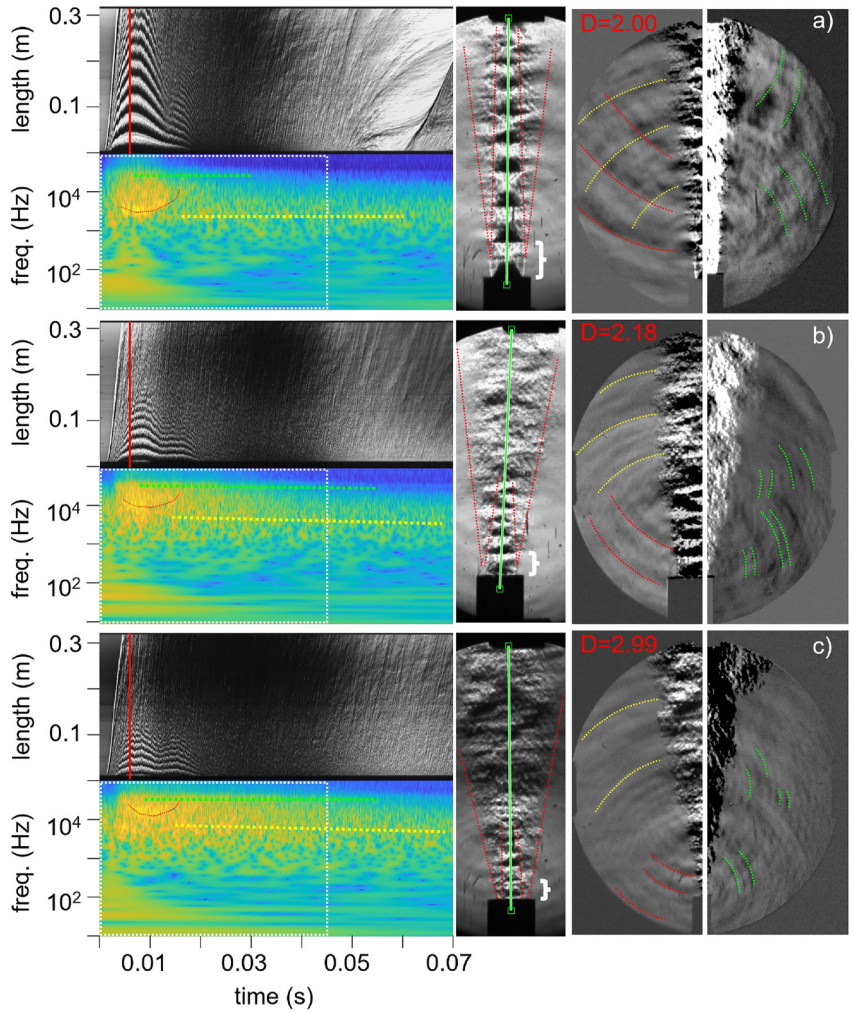

Figure 2. Acoustic and high-speed Schlieren characterization of analogue volcanic jets for smooth ($D = 2.00$), (a) or fractal ($D = 2.18$ and $D = 2.99$, (b and c) respectively) conduits at $P = 8$. Each figure shows: (i) kymographs from Schlieren high-speed videos of the experiments, showing jets evolution over time along the jet centerline line (left-hand panels, top) and the relative wavelet periodogram of the acoustic radiation with highlighted the broadband shock noise (BBSN, red), the low-frequency component of the turbulent mixing noise (TMN, yellow), and the high-frequency component of both BBSN and TMN (green) (left-hand panels, bottom, white dashed box is the time interval used to compute temporal and spectral parameters shown in Figure 4). (ii) still frame of the Schlieren high-speed video 5.3 ms after the onset of the jet (red line in kymographs), showing the supersonic jets with their shock structure (white brackets mark L_s), the jet centerline (green line), and the inner and outer boundaries of the jet shear layer (dotted red line) (central panels); and (iii) the different components of the acoustic radiation in the horizontal and vertical Schlieren projection after background subtraction (BBSN, red; TMN, yellow; high-frequency BBSN and TMN, green) (right-hand- panels). The external conduit diameter, equal to 5.3 cm, provide a spatial reference.

2.2. Analytical Methods

Acoustic and accelerometric signal processing was performed in a 0.045 s-long window encompassing the bulk of the experiment (dotted white box in Figure 2). We evaluated the RMS amplitude in the temporal domain. The temporal evolution of the spectral properties of the signals was characterized by wavelet periodograms. For each column (i.e., time step) of the periodogram (Figure 2), we extracted the frequency corresponding to the maximum spectral amplitude; then we computed the maximum frequency value obtained within the window. We also evaluated the RMS amplitude ratio between the acoustic and accelerometric signals, as a proxy for energy partitioning. For the series of experiments performed in position L and N, the pressure (p_{red}) at the reference distance (r_{red}) was obtained from the actual distance r and pressure p_x a follows (Johnson & Ripepe, 2011):

$$p_{red} = p_x * (r/r_{red}) \quad (1)$$

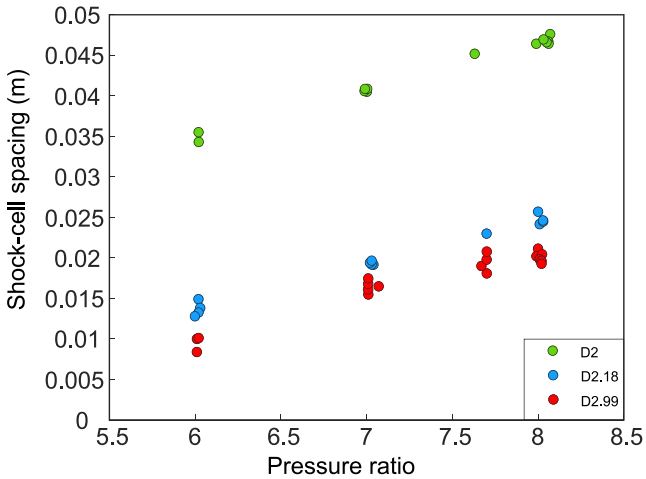

Figure 3. Shock cells spacing (L_s) as a function of pressure ratio for different conduit roughness D.

Equation 1 implies a pressure amplitude decay as $1/r$, an assumption that is valid only in the far field, that is, at distance $r >> \lambda/2\pi$, with λ defined as the acoustic wavelength. For our set of measurements performed at a source distance of $r = 1$ m, we can assume far field conditions (hence Equation 1) are valid for frequencies above 100 Hz.

The elastic emissions of the experimental jets were compared against visual observation and kymographs of the high-speed shadowgraph videos. From these, we also measured the maximum spacing between shock cells (L_s) when visible.

3. Results

Visually, the onset of the jet is marked by the propagation of acoustic waves and the formation of a vortex ring, followed by the structuring of the jet itself and its waning, according to the evolution of starting jets (Peña Fernández et al., 2020). Acoustic waves radiate first from the conduit outlet, then from the vortex ring, and finally from the jet itself (Movies S1 and S2). At $P \geq 6$ experimental jets are clearly supersonic, and the vortex ring is preceded by a shock wave and followed by the formation of an under-expanded jet with shock cells whose L_s increases for about 5 ms and then gradually decreases. In the supersonic cases, L_s and peak acoustic frequency display specular trends over time, the former increasing while the latter decreases and vice versa (Figure 2). Increasing D results also in decreasing L_s (Figure 3) and shock cell stability and in faster growth of the shear layer downstream of the jet (increasing jet spreading angle). With increasing D, the acoustic radiation in $P = 8$ experiments increases its peak frequency, and the upstream directed component decreases considerably (Figures 2 and 4, Movie S3).

Rough conduit walls leave their fingerprint also on acoustic and accelerometric signals. The RMS amplitude of both acoustic and accelerometric signals increases with increasing P. For $P > 6$ acoustic amplitude decreases

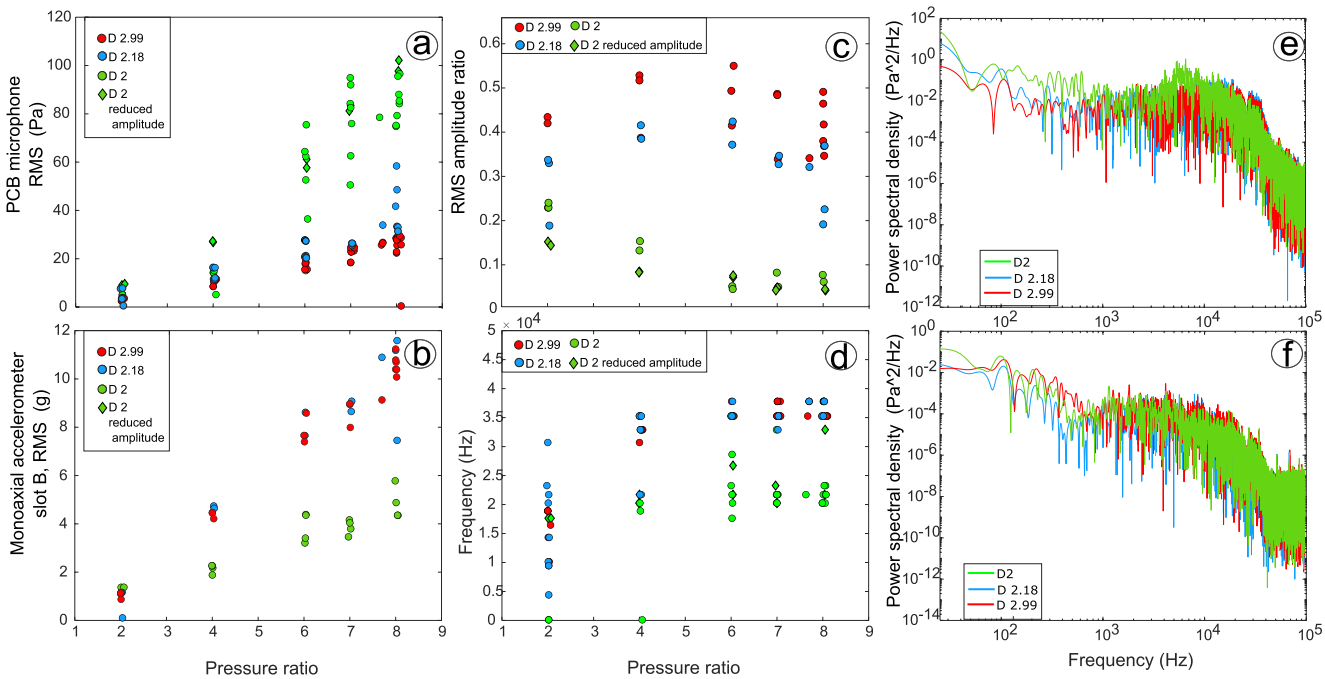

Figure 4. Acoustic and accelerometric radiation as a function of initial pressure ratio P and fractal dimension D. (a) Acoustic amplitude (RMS) of microphone in position J and L (diamonds; amplitude reduced to 30 cm); (b) accelerometric amplitude (RMS); (c) Amplitude ratio between accelerometric and acoustic radiation. (d) Peak frequency in the acoustic radiation wavelet periodogram. (e, f) Examples of Power Spectra computed using a 0.04 s window for experiments performed at $P = 8$ (e) and $P = 2$ (f).

with increasing D (Figure 4a); below this threshold the correlation is less clear. Accelerometric amplitude is always lower for $D = 2$ than for $D = 2.18$ and $D = 2.99$ (Figure 4b). The accelerometer to acoustic RMS amplitude ratio, proxy for energy partitioning between conduit and atmosphere, increases with increasing P until $P = 6$, and decreases afterward. At any P, the amplitude ratio increases with increasing D (Figure 4c).

The peak acoustic frequency of the wavelet periodograms increases with increasing D, but in a complex pattern. For $D = 2$, peak frequency increases with pressure until $P = 6$ (the approximate onset of the supersonic regime) and slightly decreases afterward, while for $D = 2.18$ and $D = 2.99$ the increase till $P = 6$ is sharper and the following decrease less marked (Figure 4d).

The effect of D is strongly nonlinear, changes in all parameters from $D = 2.00$ to $D = 2.18$ being much larger than from $D = 2.18$ to $D = 2.99$. Similar results are shown in Figure S3 in Supporting Information S1 for microphone in position Y-M and accelerometer in slot A. Figures S4 and S5 in Supporting Information S1 show examples of the temporal evolution of spectral properties of respectively acoustic and accelerometric signals at subsonic ($P = 2$) and supersonic ($P = 8$) conditions for $D = 2$.

4. Discussion

4.1. Influence of Conduit Roughness on Jet Flow Structures

Previous studies on pipe flow have shown that roughness influences heat and momentum transfer at the boundary layer by increasing pressure drop, altering laminar-turbulent transitions, inducing secondary flow motion, improving flow mixing and enhancing heat transfer (e.g., Kadivar et al., 2021 and references therein). We observed increasing accelerometric amplitude with increasing D, indicating that rougher walls increment frictional energy loss of the gas flow within conduit. Although the majority of investigations have addressed relative surface roughness (i.e., roughness height to conduit diameter; in our study ∼25% for both fractal conduits) up to 5% in percentage (e.g., Flack & Schultz, 2010; Moody, 1944; Nikuradse, 1937), research performed on micro-channels with relative roughness up to 14% highlighted the additional effect of flow area restrictions influencing pressure drop and of the increased shear stress (Kandlikar et al., 2005; Taylor et al., 2006).

The energy lost frictionally against conduit walls is partially converted into turbulent energy of the resulting starting jet. The roughness-induced frictional loss is undetectable in our setup for $P = 2$ and becomes more evident as P increases (Figure 4; Figure S3 in Supporting Information S1). The trend of the accelerometric to acoustic amplitude ratio as function of P and D reveals two key points of the conduit walls versus jet energy partition: first, it works oppositely for smooth and rough conduit walls; second, it reverses at the subsonic to supersonic transition. The first point is explained considering that, with increasing Reynolds number, friction decreases for smooth conduit and increases for rough-walled ones (Busse et al., 2017). The second point is explained by the different sources of jet noise acting in the two regimes and the respective changes in radiation directionality (e.g., Tam et al., 2008).

In the subsonic regime, turbulent mixing noise (TMN) dominates the acoustic radiation from the jet, and, in agreement with our results at $P = 2$–4, its frequency increases with Mach number (M) rising from 0.5 to 1.0 (Ilario et al., 2017). TMN has a higher frequency component mainly radiated perpendicularly from the jet direction (best visible in the vertical blade Schlieren images, in orange in Figure 2), and a lower frequency one, increasingly dominant at increasing M (in yellow in Figure 2), mainly radiating in the downstream direction (Tam, 1995), in agreement with our observations, and thus less prone to reach our microphone, located at 90° to the jet axis and level with the vent. In the supersonic regime, TMN is joined and dominated by broadband shock noise (BBSN, in red in Figure 2), due to the interaction of variably-sized, downstream-migrating jet shear layer structures with the shock cells. Screech tones were not observed in our experiments (Figures 4e and 4f; Figure S6 in Supporting Information S1), coherently with the observation that for pipes with length to diameter ratio above 6 screech tones are suppressed (e.g., Jothi & Srinivasan, 2009, 2013).

Both TMN components and BBSN are clearly visible in our Schlieren images at $P = 8$, the latter being more pronounced in the $D = 2.00$ case and radiating in the downstream direction (Figure 2 and Movies S1–S3). L_s is linked to M as follows (Norum & Seiner, 1982):

$$\frac{L_s}{D_e} = 1.1\sqrt{M^2 - 1} \tag{2}$$

where D_e is the nozzle diameter. Assuming D_e = 0.03 m (Figure 1), M in our experiments at P = 6–8 range 1.03–1.26 for D = 2.99, 1.1–1.36 for D = 2.18, and 1.6–1.99 for D = 2.00. M can be used to evaluate the jet velocity u_j according to:

$$u_j = M * c \tag{3}$$

where c is the acoustic velocity in the medium at fully expanded conditions. This allows us to evaluate the expected broadband peak frequency f_{bbsn} according to the following:

$$u_{\text{kh}} = 0.7u_j \tag{4}$$

$$f_{\text{bbsn}} = \frac{u_{\text{kh}}}{Ls} \tag{5}$$

where u_{kh} is the eddy convection velocity, computed according to Equation 4. For the observed ranges of M, according to Equation 3 u_j spans from ca. 350 m/s for D = 2.99 and P = 6 to ca. 670 m/s for D = 2.00 and P = 8 with a percentage of increase from fractal to smooth conduit with the same starting conditions of about 25% at the same P. The expected f_{bbsn} range from 8.7 * 10^3 up to 2.9 * 10^4 Hz, in relative good agreement with measured values (1 to almost 4 * 10^4 Hz, Figure 4; Figures S3 and S4 in Supporting Information S1) considering a slightly smaller nozzle diameter due to local departure from the mean values in fractal conduits.

The observed increase of f_{bbsn} with increasing D is linked with the decrease in L_s with increasing D (Figure 3), due to different contributing factors: (a) variation in the radial jet cross-section due to increasingly irregular geometry of the conduit outlet, and (b) decreasing jet velocity as gas flow interacts with increasingly rough conduit walls. In military nozzles shock-cell spacing is effectively reduced by the introduction of chevrons at the nozzle outlet, which modify initial jet cross-sectional shape by introducing counter-rotating vortex pairs into the jet (Heeb et al., 2016). Local differences in the vent roughness could modulate the initial cross-section of the jet and the subsequent shock-cell structure and shock strength in our experiments. The larger spreading angle of the jet supports the formation of a larger mixing layer and effective smaller jet diameter for larger D. Concerning jet velocity, for the same P this can be reduced by the frictional energy loss due to friction with rough conduit walls. In agreement with our observations, higher jet noise level for smooth conduit walls than for micron-scale rough conduits has been observed (Jothi & Srinivasan, 2013.). In summary, our observations in the supersonic regime are explained by increasing roughness of the conduit walls increasing the relevance of TMN at the expense of BBSN.

4.2. Implications for Volcanic Jets and Seismo-Acoustic Signals

Previous studies have highlighted the importance of conduit wall roughness on the exponent of the power law relating seismic tremor to the volume flux in experimental conduits and volcanoes, and that fractal dimension is an effective descriptor of surface topography and of magma fragmentation (Kueppers et al., 2006; Mark & Aronson, 1984; Pfeifer, 1984; Risović et al., 2009; Sciotto et al., 2019; Spina et al., 2019). In this study, we experimentally tested, for the first time, how volcanic conduit wall roughness plays a role in the amplitude and frequency of elastic (seismo-acoustic) radiation from jets, that are routinely measured during explosive eruptions (e.g., Johnson et al., 2003; Johnson & Ripepe, 2011; Rowell et al., 2014; Taddeucci et al., 2014).

The characteristic frequency of different components of subsonic to supersonic jet noise has been used to get inferences on the diameter of erupting volcanic vents and their temporal evolution (Gestrich et al., 2022; Taddeucci et al., 2021). Acoustic amplitude is an important tool to monitor jet velocity as a proxy for eruption intensity, and its link with jet noise dynamics in the volcanic environment is now established (Fee et al., 2013; Matoza et al., 2013). Here we show that changes in the frequency and amplitude of eruption-generated sound could be induced by changes in the roughness of the conduit, a fact that was previously unaccounted for, despite plenty of evidence illustrating the occurrence conduit erosion during an eruption (e.g., Aravena et al., 2017; Fee et al., 2017; Macedonio et al., 1994; Schmid et al., 2021).

For given initial conditions, smoother conduit walls or a syn-eruptive decrease in conduit roughness, resulting from erosion or lining with new magma, would result in a decrease in energy transfer to the conduit walls and a corresponding increase in jet velocity. This would significantly affect the Volcano Acoustic to Seismic Ratio (VASR; Johnson & Aster, 2005) that is the ratio among acoustic and seismic energy of a given volcanic explosion,

a parameter commonly used to characterize eruption sources and their elastic coupling with the volcano and atmosphere (e.g., Andronico et al., 2013; Johnson & Aster, 2005; Smith et al., 2020). Conduit smoothening would also translate in a change in the dominant source and directionality in the jet-related noise, different in the subsonic or supersonic regime. In the trans-sonic to supersonic regime BBSN would become more dominant and with a lower peak frequency, while in the subsonic one TMN would have a lower fine-scale turbulence component.

Our findings have implications also for the numerical modeling of the flow of gas-pyroclast mixtures in volcanic conduits, where conduit wall roughness is mostly unaccounted for (an attempt to consider conduit wall roughness for relative roughness up to 5% in magma ascent dynamics has been done by La Spina et al., 2019, 2021, 2022), and for the evolution of eruption plumes, largely controlled by jet exit velocity and air entrainment at the jet shear layer (e.g., Carey and Bursik, 2015).

5. Concluding Remarks

Experiments on the role of conduit surface roughness on flow dynamics and elastic radiation of subsonic to supersonic jets brought to light the following key points:

1. The increase in frictional energy loss with increasing roughness, inferred from the increment of accelerometric amplitude and accelerometric to acoustic amplitude ratio, is progressively more evident with increasing pressure ratio. Differences in the subsonic versus. supersonic regime for the above mentioned amplitude ratio likely mirror the contribution of distinct sources of jet noise, turbulent mixing noise dominating in the subsonic regime and broadband shock-noise in the supersonic one.
2. In the supersonic regime, decreasing shock-cell spacing with increasing roughness causes increasing acoustic frequency. This is likely to result from the decrease in jet velocity due to increased energy transfer to the conduit. The variation in the jet cross-section at the conduit outlet, possibly introducing counter-rotating vortices, represents an additional contributing factor.
3. Given that the coupling between volcanic flows and conduit shape has been shown to be highly dynamic, a wide spectrum of cross-sectional variations is expected to occur both in time and depth due to depositional and/or erosional processes. The observation of the jet structure and of the seismo-acoustic related radiation is of paramount importance for backtracking the evolution of explosive activity in conduit and to correctly interpret source processes and the coupling of their elastic energy with the conduit wall and the atmosphere.

Data Availability Statement

The repository of data is available at link: https://doi.org/10.5281/zenodo.7920109.

Acknowledgments
We thank the Editor, C. Huber and the reviewers, A. Namiki and R. Matoza for their improving comments. We also wish to thank Massimo Mari for his precious collaboration. L.S. thank the bottom up project ROUGHER funded by INGV. L.S., J.T., P.S. wish to thank the INGV-MUR Project Pianeta Dinamico—"Working Earth"—project VT—DYNAMO—2023 and the Progetto Strategico Dipartimentale INGV 2019 UNO. This project has received funding from the European Union's Horizon 2020 research and innovation programme under the Marie Sklodowska-Curie grant agreement No 101025887.

References

Andronico, D., Lo Castro, M. D., Sciotto, M., & Spina, L. (2013). The 2010 ash emissions at the summit craters of Mt Etna: Relationship with seismo-acoustic signals. *Journal of Geophysical Research: Solid Earth*, *118*(1), 51–70. https://doi.org/10.1029/2012jb009895

Aravena, Á., Vitturi, M. D. M., Cioni, R., & Neri, A. (2017). Stability of volcanic conduits during explosive eruptions. *Journal of Volcanology and Geothermal Research*, *339*, 52–62. https://doi.org/10.1016/j.jvolgeores.2017.05.003

Bridges, J., & Brown, C. (2004). Parametric testing of chevrons on single flow hot jets. In *10th AIAA/CEAS aeroacoustics conference* (p. 2824).

Busse, A., Thakkar, M., & Sandham, N. (2017). Reynolds-number dependence of the near-wall flow over irregular rough surfaces. *Journal of Fluid Mechanics*, *810*, 196–224. https://doi.org/10.1017/jfm.2016.680

Carey, M., Bursik, M., Houghton, B., James, M. R., & Vergniolle, S. (2015). Volcanic plumes. *The Encyclopedia of Volcanoes*, *571–585*. https://doi.org/10.1016/b978-0-12-385938-9.00027-4

Cigala, V., Kueppers, U., Peña Fernández, J. J., Taddeucci, J., Sesterhenn, J., & Dingwell, D. B. (2017). The dynamics of volcanic jets: Temporal evolution of particles exit velocity from shock-tube experiments. *Journal of Geophysical Research: Solid Earth*, *122*(8), 6031–6045. https://doi.org/10.1002/2017jb014149

Davies, T. P. (1981). Schlieren photography—Short bibliography and review. *Optics & Laser Technology*, *13*(1), 37–42. https://doi.org/10.1016/0030-3992(81)90089-X

Fee, D., Haney, M. M., Matoza, R. S., Van Eaton, A. R., Cervelli, P., Schneider, D. J., & Iezzi, A. M. (2017). Volcanic tremor and plume height hysteresis from Pavlof Volcano, Alaska. *Science*, *355*(6320), 45–48. https://doi.org/10.1126/science.aah6108

Fee, D., Matoza, R. S., Gee, K. L., Neilsen, T. B., & Ogden, D. E. (2013). Infrasonic crackle and supersonic jet noise from the eruption of Nabro Volcano, Eritrea. *Geophysical Research Letters*, *40*(16), 4199–4203. https://doi.org/10.1002/grl.50827

Flack, K. A., & Schultz, M. P. (2010). Review of hydraulic roughness scales in the fully rough regime. *Journal of Fluids Engineering*, *132*(4). https://doi.org/10.1115/1.4001492

Genco, R., Ripepe, M., Marchetti, E., Bonadonna, C., & Biass, S. (2014). Acoustic wavefield and Mach wave radiation of flashing arcs in strombolian explosion measured by image luminance. *Geophysical Research Letters*, *41*(20), 7135–7142. https://doi.org/10.1002/2014gl061597

George, W. K. (1989). The self-similarity of turbulent flows and its relation to initial conditions and coherent structures. In R. E. A. Arndt & W. K. George (Eds.), *Recent advances in turbulence* (p. 3973). Hemisphere.
Gestrich, J. E., Fee, D., Matoza, R. S., Lyons, J. J., Dietterich, H. R., Cigala, V., et al. (2022). Lava fountain jet noise during the 2018 eruption of fissure 8 of Kīlauea volcano. *Frontiers of Earth Science*, *10*, 1027408. https://doi.org/10.3389/feart.2022.1027408
Giudicepietro, F., Esposito, A. M., Spina, L., Cannata, A., Morgavi, D., Layer, L., & Macedonio, G. (2021). Clustering of experimental seismo-acoustic events using self-organizing map (SOM). *Frontiers in Earth Science*, *8*, 581742. https://doi.org/10.3389/feart.2020.581742
Goto, A., Ripepe, M., & Lacanna, G. (2014). Wideband acoustic records of explosive volcanic eruptions at Stromboli: New insights on the explosive process and the acoustic source. *Geophysical Research Letters*, *41*(11), 3851–3857. https://doi.org/10.1002/2014gl060143
Haney, M. M., Matoza, R. S., Fee, D., & Aldridge, D. F. (2018). Seismic equivalents of volcanic jet scaling laws and multipoles in acoustics. *Geophysical Journal International*, *213*(1), 623–636. https://doi.org/10.1093/gji/ggx554
Heeb, N., Gutmark, E., & Kailasanath, K. (2016). Impact of chevron spacing and asymmetric distribution on supersonic jet acoustics and flow. *Journal of Sound and Vibration*, *370*, 54–81. https://doi.org/10.1016/j.jsv.2016.01.047
Ilário, C. R., Azarpeyvand, M., Rosa, V., Self, R. H., & Meneghini, J. R. (2017). Prediction of jet mixing noise with Lighthill's Acoustic Analogy and geometrical acoustics. *Journal of the Acoustical Society of America*, *141*(2), 1203–1213. https://doi.org/10.1121/1.4976076
Johnson, J. B., & Aster, R. C. (2005). Relative partitioning of acoustic and seismic energy during Strombolian eruptions. *Journal of Volcanology and Geothermal Research*, *148*(3–4), 334–354. https://doi.org/10.1016/j.jvolgeores.2005.05.002
Johnson, J. B., Aster, R. C., Ruiz, M. C., Malone, S. D., McChesney, P. J., Lees, J. M., & Kyle, P. R. (2003). Interpretation and utility of infrasonic records from erupting volcanoes. *Journal of Volcanology and Geothermal Research*, *121*(1–2), 15–63. https://doi.org/10.1016/s0377-0273(02)00409-2
Johnson, J. B., & Ripepe, M. (2011). Volcano infrasound: A review. *Journal of Volcanology and Geothermal Research*, *206*(3–4), 61–69. https://doi.org/10.1016/j.jvolgeores.2011.06.006
Jothi, T. J. S., & Srinivasan, K. (2009). Role of initial conditions on noise from underexpanded pipe jets. *Physics of Fluids*, *21*(6), 066103. https://doi.org/10.1063/1.3153909
Jothi, T. J. S., & Srinivasan, K. (2013). Surface roughness effects on noise from pipe jets. *Journal of Sound and Vibration*, *332*(4), 839–849. https://doi.org/10.1016/j.jsv.2012.10.001
Kadivar, M., Tormey, D., & McGranaghan, G. (2021). A review on turbulent flow over rough surfaces: Fundamentals and theories. *International Journal of Thermofluids*, *10*, 100077. https://doi.org/10.1016/j.ijft.2021.100077
Kandlikar, S. G., Schmitt, D., Carrano, A. L., & Taylor, J. B. (2005). Characterization of surface roughness effects on pressure drop in single-phase flow in minichannels. *Physics of Fluids*, *17*(10), 100606. https://doi.org/10.1063/1.1896985
Kueppers, U., Perugini, D., & Dingwell, D. B. (2006). Explosive energy during volcanic eruptions from fractal analysis of pyroclasts. *Earth and Planetary Science Letters*, *248*(3–4), 800–807. https://doi.org/10.1016/j.epsl.2006.06.033
La Spina, G., Arzilli, F., Burton, M. R., Polacci, M., & Clarke, A. B. (2022). Role of volatiles in highly explosive basaltic eruptions. *Communications Earth and Environment*, *3*(1), 156. https://doi.org/10.1038/s43247-022-00479-6
La Spina, G., Arzilli, F., Llewellin, E. W., Burton, M. R., Clarke, A. B., Vitturi, M. D. M., et al. (2021). Explosivity of basaltic lava fountains is controlled by magma rheology, ascent rate and outgassing. *Earth and Planetary Science Letters*, *553*, 116658. https://doi.org/10.1016/j.epsl.2020.116658
La Spina, G., Clarke, A. B., Vitturi, M. D. M., Burton, M., Allison, C. M., Roggensack, K., & Alfano, F. (2019). Conduit dynamics of highly explosive basaltic eruptions: The 1085 CE Sunset Crater sub-Plinian events. *Journal of Volcanology and Geothermal Research*, *387*, 106658. https://doi.org/10.1016/j.jvolgeores.2019.08.001
Macedonio, G., Dobran, F., & Neri, A. (1994). Erosion processes in volcanic conduits and application to the AD 79 eruption of Vesuvius. *Earth and Planetary Science Letters*, *121*(1–2), 137–152. https://doi.org/10.1016/0012-821x(94)90037-x
Mark, D. M., & Aronson, P. B. (1984). Scale-dependent fractal dimensions of topographic surfaces: An empirical investigation, with applications in geomorphology and computer mapping. *Journal of the International Association for Mathematical Geology*, *16*(7), 671–683. https://doi.org/10.1007/bf01033029
Matoza, R. S., Arciniega-Ceballos, A., Sanderson, R. W., Mendo-Pérez, G., Rosado-Fuentes, A., & Chouet, B. A. (2019). High-broadband seismoacoustic signature of Vulcanian explosions at Popocatépetl volcano, Mexico. *Geophysical Research Letters*, *46*(1), 148–157. https://doi.org/10.1029/2018GL080802
Matoza, R. S., Chouet, B. A., Jolly, A. D., Dawson, P. B., Fitzgerald, R. H., Kennedy, B. M., et al. (2022). High-rate very-long-period seismicity at Yasur volcano, Vanuatu: Source mechanism and decoupling from surficial explosions and infrasound. *Geophysical Journal International*, *230*(1), 392–426. https://doi.org/10.1093/gji/ggab533
Matoza, R. S., Fee, D., Garcés, M. A., Seiner, J. M., Ramon, P. A., & Hedlin, M. A. H. (2009). Infrasonic jet noise from volcanic eruptions. *Geophysical Research Letters*, *36*(8), L08303. https://doi.org/10.1029/2008gl036486
Matoza, R. S., Fee, D., Neilsen, T. B., Gee, K. L., & Ogden, D. E. (2013). Aeroacoustics of volcanic jets: Acoustic power estimation and jet velocity dependence. *Journal of Geophysical Research: Solid Earth*, *118*(12), 6269–6284. https://doi.org/10.1002/2013jb010303
Mi, J., Nobes, D. S., & Nathan, G. J. (2001). Influence of jet exit conditionns on the passive scalar field of an axisymmetric free jet. *Journal of Fluid Mechanics*, *432*, 91–125. https://doi.org/10.1017/s0022112000003384
Moody, L. F. (1944). Friction factors for pipe flow. *Transactions of the American Society of Mechanical Engineers*, *66*(8), 671–678. https://doi.org/10.1115/1.4018140
Nikuradse, J. (1937). *Laws of flows in rough pipes* (p. 129). Technical Memorandum.
Norman, M. L., & Winkler, K. H. A. (1985). Los Alamos Science. Los Alamos National Laboratory, Los Alamos 12, 38.
Norum, T. D., & Seiner, J. M. (1982). Broadband shock noise from supersonic jets. *AIAA Journal*, *20*(1), 68–73. https://doi.org/10.2514/3.51048
Peña Fernández, J., & Sesterhenn, J. (2017). Compressible starting jet: Pinch-off and vortex ring–trailing jet interaction. *Journal of Fluid Mechanics*, *817*, 560–589. https://doi.org/10.1017/jfm.2017.128
Peña Fernández, J. J., Cigala, V., Kueppers, U., & Sesterhenn, J. (2020). Acoustic analysis of starting jets in an anechoic chamber: Implications for volcano monitoring. *Scientific Reports*, *10*(1), 13576. https://doi.org/10.1038/s41598-020-69949-1
Pfeifer, P. (1984). Fractal dimension as working tool for surface-roughness problems. *Applications of Surface Science*, *18*(1–2), 146–164. https://doi.org/10.1016/0378-5963(84)90042-4
Prejean, S. G., & Brodsky, E. E. (2011). Volcanic plume height measured by seismic waves based on a mechanical model. *Journal of Geophysical Research*, *116*(B1), B01306. https://doi.org/10.1029/2010jb007620
Risović, D., Poljaček, S. M., & Gojo, M. (2009). On correlation between fractal dimension and profilometric parameters in characterization of surface topographies. *Applied Surface Science*, *255*(7), 4283–4288. https://doi.org/10.1016/j.apsusc.2008.11.028

Rowell, C. R., Fee, D., Szuberla, C. A. L., Arnoult, K., Matoza, R. S., Firstov, P. P., et al. (2014). Three-dimensional volcano-acoustic source localization at Karymsky volcano, Kamchatka, Russia. *Journal of Volcanology and Geothermal Research*, *283*, 101–115. https://doi.org/10.1016/j.jvolgeores.2014.06.015

Schmid, M., Kueppers, U., Cigala, V., & Dingwell, D. B. (2022). Complex geometry of volcanic vents and asymmetric particle ejection: Experimental insights. *Bulletin of Volcanology*, *84*(8), 71. https://doi.org/10.1007/s00445-022-01580-6

Schmid, M., Kueppers, U., Civico, R., Ricci, T., Taddeucci, J., & Dingwell, D. B. (2021). Characterising vent and crater shape changes at Stromboli: Implications for risk areas. *Volcanica*, *4*(1), 87–105. https://doi.org/10.30909/vol.04.01.87105

Sciotto, M., Cannata, A., Prestifilippo, M., Scollo, S., Fee, D., & Privitera, E. (2019). Unravelling the links between seismo-acoustic signals and eruptive parameters: Etna lava fountain case study. *Scientific Reports*, *9*(1), 1–12. https://doi.org/10.1038/s41598-019-52576-w

Smith, C. M., Thompson, G., Reader, S., Behnke, S. A., McNutt, S. R., Thomas, R., & Edens, H. (2020). Examining the statistical relationships between volcanic seismic, infrasound, and electrical signals: A case study of Sakurajima volcano, 2015. *Journal of Volcanology and Geothermal Research*, *402*, 106996. https://doi.org/10.1016/j.jvolgeores.2020.106996

Spina, L., Cannata, A., Morgavi, D., & Perugini, D. (2019). Degassing behaviour at basaltic volcanoes: New insights from experimental investigations of different conduit geometry and magma viscosity. *Earth-Science Reviews*, *192*, 317–336. https://doi.org/10.1016/j.earscirev.2019.03.010

Spina, L., Cannata, A., Morgavi, D., Privitera, E., & Perugini, D. (2022). Seismo-acoustic gliding: An experimental study. *Earth and Planetary Science Letters*, *579*, 117344. https://doi.org/10.1016/j.epsl.2021.117344

Swanson, E., Theunissen, R., Rust, A., Green, D., & Phillips, J. (2018). An experimental study of the flow structure and acoustics of jets: Implications for volcano infrasound. *Journal of Volcanology and Geothermal Research*, *363*, 10–22. https://doi.org/10.1016/j.jvolgeores.2018.08.005

Taddeucci, J., Peña Fernández, J. J., Cigala, V., Kueppers, U., Scarlato, P., Del Bello, E., et al. (2021). Volcanic vortex rings: Axial dynamics, acoustic features, and their link to vent diameter and supersonic jet flow. *Geophysical Research Letters*, *48*(15), e2021GL092899. https://doi.org/10.1029/2021gl092899

Taddeucci, J., Scarlato, P., Capponi, A., Del Bello, E., Cimarelli, C., Palladino, D. M., & Kueppers, U. (2012). High-speed imaging of Strombolian explosions: The ejection velocity of pyroclasts. *Geophysical Research Letters*, *39*(2), L02301. https://doi.org/10.1029/2011gl050404

Taddeucci, J., Sesterhenn, J., Scarlato, P., Stampka, K., Del Bello, E., Pena Fernandez, J. J., & Gaudin, D. (2014). High-speed imaging, acoustic features, and aeroacoustic computations of jet noise from Strombolian (and Vulcanian) explosions. *Geophysical Research Letters*, *41*(9), 3096–3102. https://doi.org/10.1002/2014gl059925

Tam, C. K. (1995). Supersonic jet noise. *Annual Review of Fluid Mechanics*, *27*(1), 17–43. https://doi.org/10.1146/annurev.fl.27.010195.000313

Tam, C. K., Viswanathan, K., Ahuja, K. K., & Panda, J. (2008). The sources of jet noise: Experimental evidence. *Journal of Fluid Mechanics*, *615*, 253–292. https://doi.org/10.1017/S0022112008003704

Taylor, J. B., Carrano, A. L., & Kandlikar, S. G. (2006). Characterization of the effect of surface roughness and texture on fluid flow—Past, present, and future. *International Journal of Thermal Sciences*, *45*(10), 962–968. https://doi.org/10.1016/j.ijthermalsci.2006.01.004

Wilson, L. (1976). Explosive volcanic eruptions—III. Plinian eruption columns. *Geophysical Journal International*, *45*(3), 543–556. https://doi.org/10.1111/j.1365-246x.1976.tb06909.x

References From the Supporting Information

Bunjong, D., Pussadee, N., & Wattanakasiwich, P. (2018). Optimized conditions of Schlieren photography. *Journal of Physics: Conference Series*, *1144*, 012097. https://doi.org/10.1088/1742-6596/1144/1/012097

Gopal, V., Klosowiak, J. L., Jaeger, R., Selimkhanov, T., & Hartmann, M. J. Z. (2008). Visualizing the invisible: The construction of three low-cost schlieren imaging systems for the undergraduate laboratory. *European Journal of Physics*, *29*(3), 607–617. https://doi.org/10.1088/0143-0807/29/3/020